MINISTRY OF EDUCATION AND TRAINING
NHA TRANG UNIVERSITY

HO HUU HUY

RESEARCH ON STRENGTHS AND FAILURE BEHAVIOR OF THE DISSIMILAR FRICTION WELDING BETWEEN ALUMINUM ALLOY AA6061-T6 AND STAINLESS STEEL SUS316

Mayor: Mechanical Engineering

Major code: 9520103

DOCTOR OF PHILOSOPHY THESIS ABSTRACT

KHANH HOA - 2025

The thesis was completed at Nha Trang University

Supervisors: **1. Associate Professor Ph.D.Tran Hung Tra**

2. Associate Professor Ph.D.Duong Dinh Hao

Reviewer 1: Associate Professor Ph.D.Dang Quoc Khanh

Reviewer 2: Associate Professor Ph.D.Vu Cong Hoa

The thesis was defended at the school level at Nha Trang University at 14h, on 17 month 5 year 2025.

Thesis can be found at: National library and Nha Trang University library.

INTRODUCTION

1. Reasons for choosing the thesis of FSWed AA6061/SUS316

AA6061-T6 and SUS316 according to JIS standards are materials with wide applications in industries including aerospace, shipbuilding, marine structures, automotive, construction and machinery. Research into welding between materials help to improve quality and amount for these industries.

Structure optimization: AA6061-T6 are lightweight and high strength, while SUS316 are corrosion and heat resistance. Combining these materials can create structures with superior performance.

Solving the challenges in bonding dissimilar materials: Welding aluminum and stainless steel is a major technical challenge due to the differences in physical and chemical properties. Aluminum is low melting point and is oxidized easily. In that case, stainless steel is oxidation resistance but difficult to weld with aluminum. Research helps solve technical problems in welding process so improving the quality and durability of the joint.

Contribution to academic: Currently, there are very few studies on the failure and corrosion mechanism of FSWed AA6061-T6/SUS316 joint in different corrosion environments. Research on this subject not only contributes to scientific knowledge but also provides theoretical and practical for the design and manufacture products with high quality weld.

Contribute to economic development and environmental protection: Better known of the corrosion mechanisms can improve corrosion resistance, extend service and reduce maintenance cost. This not only brings economic benefits but also contributes to environmental protection and safety for the industrial.

Contribute to the development and application of welding technology: This study may open up new directions in welding technology, especially of advanced welding techniques such as friction stir welding. The results can be applied to improve welding process and develop more efficient welding method.

2. Research objectives

Research objective of the topic: To determine the destructive behavior of FSW between AA6061-T6 aluminum alloy and SUS316 stainless steel fabricated by different

rotation, welding speed, penetration, pin lengths. In addition, the destruction of the lap-joint due to corrosion under the impact of different environments are also clarified.

3. Research object

- Tensile strength, destructive behavior and influence of welding parameters.
- Mechanism of the lap-joint's failure in different corrosive environments.

4. Research scope

- Lap-joint between AA6061-T6 (thickness of 3.0 mm) and SUS316 (thickness of 1.0 mm) by FSW technology.
- Study of microhardness of lap-joint.
- Study on the influence of rotation speed, welding speed, penetration and pin length on the microstructure, microhardness and mechanical properties.
- Study on the influence of different corrosive environments including: %NaCl, %NaCl + voltage, %NaCl + voltage + temperature on the corrosion process.

5. Scientific research method

5.1. Theoretical research

Synthesize published domestic and foreign research results as a basis for inheriting and approaching content related to the thesis.

5.2. Experimental research

- Fabrication of the lap-joint between AA6061-T6 and SUS316 at the FSW lab in Nha Trang University.
- Manufacturing specimens according to ASTM standards for structural investigation, microhardness testing.
- Determine the structure zone including: grain structure, IMC and diffusion thickness, surface morphology of the interface between AA6061-T6 and SUS316.
- Experimental specimens in the different corrosive environments including: %NaCl, %NaCl + voltage, %NaCl + voltage + temperature on corrosion process.

6. Scientific and practical significance of the thesis

6.1. Scientific significance

Academic contributions in the dissimilar joint: This study provides a better understanding of the dissimilar alloy welding mechanism. The optimum quality corresponding to the welding parameters help to understand the FSWed joint, the interaction between the chemical and physical components, contribution to materials science.

Contribute to the development of new material technology: Research and analysis of the weld mechanism between aluminum alloys and stainless steel may lead to the improvement of new welding techniques. These techniques can be applied in many industries, helping to improve product quality and production efficiency.

Elucidating the corrosion mechanism and the premise for prevention: Studying the corrosion mechanism in the different corrosive environments (NaCl, voltage, temperature) helps to better understand the mechanism of electrochemical corrosion and how to prevent it. This provides the knowledge need to develop corrosion protection when aluminum/stainless steel hybrid operate in the corrosive environments. Thereby increasing the durability and life of FSW products.

Scientific basis for further research: Results provide scientific data on mechanical, chemical and microstructural properties of the AA6061-T6/SUS316 lap-joint. The data can be used as reference for future research and application in practice industries.

6.2. Practical significance

Contribute to improving manufacturing efficiency: Understanding the welding mechanism between AA6061-T6 and SUS316 in particular and friction stir welding in general can lead to improved manufacturing processes, helping to increase efficiency and reduce costs. FSW technique can be applied to manufacture products with better quality at low cost.

Improve durability and equipment life: Research helps to find optimal welding methods and effective anti-corrosion measures, so increasing the durability and lifespan of products between aluminum alloy and stainless steel by FSW, especially aerospace, shipbuilding, marine structures and automotive industries.

Opening up development directions for key industries: Friction stir welding between aluminum alloys and stainless steel can be applied in the aerospace industry where materials are required lightweight but high strength or in the automotive industry to reduce weight and improve fuel efficiency.

Development of high tech products: The research can be applied to high tech products such as medical devices, electronic components,... where products are required high aesthetics and performance.

Save materials and energy: FSW technique use low energy, no welding rod, gas, or protective flux. Efficient welding techniques reduce waste material, energy consumption, adverse environmental impacts and lower cost.

CHAPTER 1. OVERVIEW

1.1. Method of bonding aluminum alloy and steel

There are many welding methods to join alloys together, including: arc welding, gas metal arc welding, submerged arc welding, resistance spot welding,… and others.

Light weight equipment and structures are a top goal in technology fields. The huge difference in physical and chemical properties make Al and Fe unstable, especially aluminum and steel don't bond successfully by fusion welding method. Currently, researchers have used to make between aluminum alloy and steel by FSW.

1.2. Potential of FSW technology

The FSW technology is one of the solid state welding techniques. FSW has emerged as an outstanding technology for welding aluminum alloys and steel, offering high strength and long durability. As of now, some domestic research has only focused on creating FSW between aluminum alloys. Mai Dang Tuan tested butt joint of 6061 aluminum. Duong Dinh Hao et al. have examined parameters affecting the structure and tensile strength of the AA7075 joint. Besides, Phan Thanh Nhan et al. fabricated the AA5083 T-shaped successfully by FSW technology.

Globally, the joining of aluminum alloys with steel using friction welding technology has been extensively researched and applied. FSW is being used to weld different alloys that traditional molten welding methods cannot perform. A large number of studies have investigated the effects of rotational speed, welding speed, and penetration on the microstructure and mechanical properties of the joint between aluminum alloys and steel. Furthermore, these parameters also influence the formation of IMC and the diffusion layer. The formation of IMC is observed commonly in joint between different materials due to the diffusion of metallic elements. Determining the correlation between rotational speed, welding speed and the resulting mechanical properties of the joint is essential for achieving optimal performance.

1.3. Applications of aluminum alloys and stainless steel in engineering

1.3.1. Aluminum alloys

Aluminum alloy is lightweight, silver gray and good oxidation resistance. Oxidizing properties of aluminum increase corrosion resistance in the atmospheric. 2xxx aluminum alloy is used in the aerospace, transportation and sport industries. 5xxx aluminum alloy is

the group with the best durability and corrosion resistance among the non-heat-treatable aluminum alloy, used in the shipbuilding, transportation, pressure tanks and bridges widely. 6xxx and 7xxx aluminum alloys are used to process heavy load parts and work in the high humidity environments such as aircraft, aerospace. Most aluminum alloys are difficult to join by welding, especially the 2xxx and 7xxx aluminum alloy. Nowadays, friction welding method is considered for welding all aluminum effectively.

1.3.2. Stainless steel

Stainless steel is a steel containing at least 10.5 % chromium, with the addition of nickel. Ferritic steel is used in architecture and household appliances commonly. Stainless steel is acid resistant and does not shrink at 1100 ^{o}C, making it a popular material for oil and gas equipment. In addition, stainless steel is manufactured equipment for transporting and storing liquefied gas, which can withstand -196 ^{o}C. With corrosion resistance, it is used to manufacture the frame for solar panel.

1.4. Some bonding techniques between aluminum and stainless steel

Current, the methods of joining aluminum and steel are used include: laser welding, resistance welding, rivet and friction stir welding. When using the MIG welding, lap-joint between aluminum and stainless steel is porous, unevenly, so it is necessary to choose the appropriate voltage to achieve the highest tensile strength.

To limit the formation of brittle layer, solid state welding methods have been applied such as resistance spot welding, laser and ultrasonic welding. Disadvantages of resistance spot welding include energy consumption and electrode wear. The joint between aluminum and steel by laser welding will form thick intermetallic compounds which is disadvantage for the joint and cannot be applied to thin sheets. Friction stir welding and friction crush welding are mixing particles well and therefore tensile strength higher than MIG welding.

Currently, research on FSW between AA6061-T6 and SUS316 still has many limitations, specifically:

- Domestically: FSW between AA6061-T6 and SUS316 is an entirely new problem and has not been researched yet.

- Foreign research on the butt welding of aluminum alloy and stainless steel using the MIG welding method shows the following results: The joints are rough with shallow penetration, and the weld strength is about 20 % of the initial strength of the aluminum

alloy. The strength of the weld is higher, around 50 % of the aluminum alloy's strength, when using friction stir welding, but the weld is not straight and has significant slag. Mahto R.P. et al. (2016) studied the microstructure of the AA6061/AISI304 joint, revealing the presence of IMC such as Fe_2Al_5 and Fe_4Al_{13}. Newishy M. et al. (2023) investigated the microstructure of the AA6061/SUS316 joint, identifying the presence of $FeAl_3$ and $FeAl_6$ compounds in the IMC layer. The steel grain size in AA6061 is large, reaching 6 μm. Zheng Q. et al. (2016) researched tensile strength of the AA6061/SUS316 butt joint using a Zn interlayer. Zin reduces the formation of IMC, improving the weld strength to 28 % of the original aluminum alloy's strength. Xingbin H. and et al. (2024) annealed SUS316 at 800 °C. As a result, tensile strength of the AA6061/SUS316 butt joint increased approximately 14.5 % due to the reduced thickness of the brittle $FeAl_3$ IMC layer, enhancing the joint's durability.

These findings provide valuable insights into the factors affecting the quality and tensile strength of aluminum alloys and stainless steel joint, which can help optimize the welding process. The studies primarily focus on investigating the impact of IMC layer on tensile strength, but have not delved deeply into the failure mechanisms. Therefore, the objective of the topic is to “Investigate the strength and failure mechanisms of friction stir welded joints between AA6061-T6 and SUS316.”

1.5. Application of aluminum and steel hybrid structures

Nowadays, saving fuel and reducing CO_2 emissions are concerts of automobile manufacturers. Aluminum alloy is combined with stainless steel in the hull and other structures to enhance resistance to corrosion, reduce weight. In addition, the aluminum alloy/stainless steel hybrid helps optimize the structure of the aircraft frame, reducing overall weight and increasing durability. Interior decoration such as railings, doors and other lightweight structure use aluminum/steel hybrid to provide aesthetics, durability and reduce costs. Food processing equipment uses the aluminum/stainless steel hybrid to ensure hygiene, corrosion resistance and durability. Aluminum/steel structures are applied in the energy production. In addition, medical equipment such as operating tables, hospital beds and other medical instruments are manufactured between aluminum alloy and stainless steel to ensure corrosion resistance, clean easy and high durability. Exoskeletons and other weight bearing devices use this combination to ensure biocompatibility and durability.

1.6. Challenges in welding between stainless steel and aluminum alloys

The melting point of the two alloys is quite different, so the coefficient of thermal expansion is different. The diverse crystal lattice structure makes it to bond together difficult by fusion welding. In addition, brittle intermetallic compounds such as $FeCl_2$, $FeCl_3$, Fe_2Al_5... at the interface leading to cracks of the joint. Al_2O_3 oxide film is formed on the surface of aluminum alloy easily when subjected to friction heat so the mechanical properties of the joint is reduced. When using fusion welding, the joint often exhibit numerous defects such as slag inclusions, hot cracks, cold cracks, a brittle heat-affected zone, residual stresses, and significant deformation. These factors lead to low tensile strength and reduced service life. Additionally, fusion welding consumes electricity, intermediary materials, and generates waste. The welding fumes produced can be harmful to workers' health and contribute to environmental pollution.

CHAPTER 2. THEORETICAL BASIS

2.1. Overview of FSW technology

2.1.1. Friction stir welding principle

FSW with basic principle: the welding tool rotates, bears axial force so it contacts and penetrates into the workpiece slowly to form friction heat (Fig. 2.1)

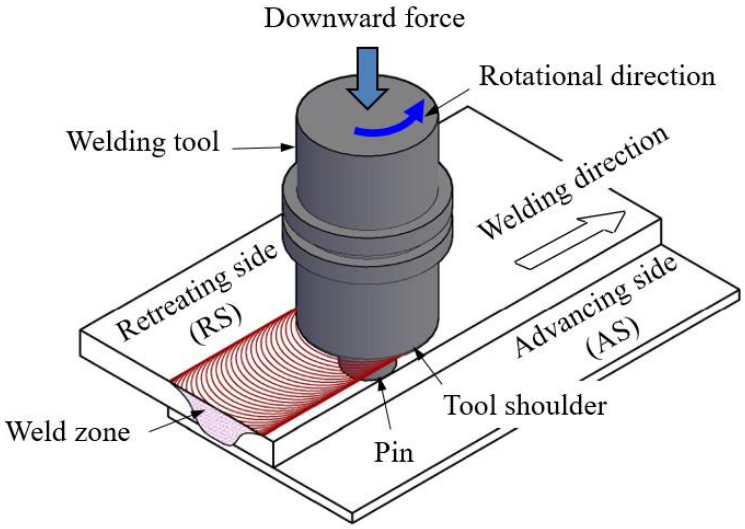

Fig. 2.1. Diagram illustrating the FSW process

The welding tool penetrates workpiece and causes plastic deformation in the stirring zone so change the structure of the material. The welding tool move along welding direction will form the joint. The welding tool has both heating the workpiece and moving, pressing the material, while preventing material out of the shoulder. Friction stir welding can be performed for many different types: butt, lap, T - welding…

2.1.2. Advantages and disadvantages of FSW

2.1.2.1. Advantages

- No filler material, no gas or welding flux. Firction stir welding saves energy, do not produce smoke, spatter or arc sparks.

- The joint has less deformation, residual stress and fewer defects. The IMC thickness at interface is smaller than fusion welding.

- Welding of dissimilar alloys results in superior strength and longevity.

2.1.2.2. Disadvantages

- The downward force is large, so the machine base must be durable. Weld the complex profiles are difficult.

- Low friction stir welding accessibility due to high equipment cost.

- Pin hole appear at the end of the joint.

2.1.3. Temperature distribution, material flow and structure zone

2.1.3.1. Temperature distribution, material flow

The FSW process includes three phenomena: heating, plastic deformation and cooling process. The material undergoes strong plastic at high temperatures, form fine grains and recrystallization resulting in good mechanical properties. The tool heats workpiece and moves the material to form the joint. High rotation speed, low welding speed are high heat welding and vice versa. High temperature lead to thick and brittle intermetallic compounds, so the mechanical properties of the joint are reduced. Low temperatures, internal defects in the joint often appear. Both low or high heat welding cause defects.

2.1.3.2. Structure zone

The weld structure zone is shown in Fig. 2.2, three zone: Heat affected zone (HAZ), thermo mechanically affected zone (TMAZ) and stir zone (SZ). SZ has the largest deformation material. TMAZ next to SZ so temperature is lower. Temperature at the HAZ is lower than SZ and TMAZ.

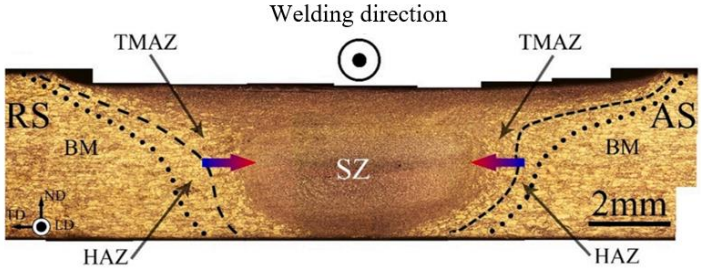

Fig. 2.2. Weld structure zone

2.1.4. Welding parameters

- Downward force F_z (P): is the main axial compressive force, pressing the material into the joint, reducing cracks and porosity defects.

- Welding tool tilt angle θ: Proper tilt angle prevents material from protruding out of the welding tool shoulder.

- Rotation speed ω: Counterclockwise or clockwise rotation will create frictional heat, softening the material around the welding tool.

- Welding speed v: Along with the rotation speed, during the movement, the welding tool softens the material.

- Pin length L: is one of the parameters affecting the quality of the joint, related to stirring and mixing the materials.

2.2. Properties of the IMC between steel and aluminum

2.2.1. Composition of IMC, formation and development mechanism

Microstructure of the interface is not smooth due to the α-Fe (ferit) grains and the thin intermetallic compounds Fe_xAl_y by chemical reactions and diffusion between Al and Fe particles. Diffusion time and chemical composition are two major factors influencing the formation of IMC during welding aluminum/steel. Al-rich of the IMC form a less ductile and stiffer joint than Fe-rich of the IMC. In the Fe - Al phase, depending on the heat input, two types of IMC are seen including Fe-rich phase (Fe_3Al and FeAl) and Al-rich phase (Fe_2Al_5, $FeAl_2$ and $FeAl_3$). Fe-rich of the IMC between aluminum and steel such as $AlCrFe_2$, AlFe, $Al_{13}Fe_4$ of AA6061/AISI304 lap-joint.

2.2.2. Prediction of IMC thickness

According to published studies, especially FSW between AA60601 and stainless steel, the IMC thickness varies from 0.34 μm to 5.5 μm. Thickness of the IMC changes according to the rotation speed, welding speed, penetration and pin length, so the diffusion also changes accordingly.

2.3. Electrochemical corrosion of dissimilar alloys joint

The redox reaction between the material and the electrolyte environment is called electrochemical corrosion. Two dissimilar alloys in electrolyte form a galvanic cell, the ions move between two electrodes generates an electric current.

On the surface, there are anode and cathode regions due to the difference in electrode potential of different alloys.

- The metal dissolved at the anode undergoes oxidation: $Me - Ze \rightarrow Me^{Z+}$
- Dissolved oxygen in solution at the cathode: $\frac{Z}{4}O_2 + Ze + ZH^+ \rightarrow \frac{Z}{2}H_2O$

$2H^+ + 2e \rightarrow H_2$.

Al has a more negative electrode than Fe, so AA6061-T6 corrodes. Thermomechanical action of the FSW process changes the microstructure, mechanical and electrochemical properties. The thermomechanical process affects local corrosion such as pitting corrosion and interfacial corrosion. In addition, the grain microstructure in different zones, forming localized electrochemical corrosion cells. Rotation speed and welding speed affect corrosion rate of the joint.

The AA6061-T6/SUS316 joint, when exposed to NaCl electrolyte solution, undergoes electrochemical corrosion. Corrosion reactions A are predicted as follows:

- Anode (Oxidation reaction): At the anode, iron (Fe) in the stainless steel (SUS316) is oxidized into Fe^{2+} ions and releases electrons (e^-): $2Fe \rightarrow 2Fe^{2+} + 4e$.

- Cathode (Reduction reaction): At the cathode, the electrons are absorbed and participate in the reduction of oxygen and protons: $O_2 + 2H_2O + 4e^- \rightarrow 4OH$

$$2H^+ + 2e = H_2$$

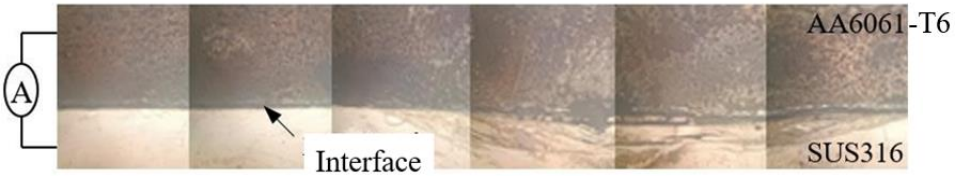

Figure 2.3. Electrochemical corrosion diagram of AA6061-T6/SUS316 joint

In addition, AA6061-T6 reacts strongly with H_2O, forming a passive oxide layer, $Al(OH)_3$, on the surface of the weld during the corrosion process. This oxide layer helps protect the AA6061-T6 from further corrosion by acting as a barrier, although its effectiveness can be affected by the presence of corrosive agents, such as chloride ions in NaCl solution.

$$2Al + 6H_2O \rightarrow 2Al(OH)_3 + 3H_2$$

The $Al(OH)_3$ oxide layer that forms on AA6061-T6 provides a protective barrier, preventing direct contact between AA6061-T6 and the NaCl solution, thus giving it high corrosion resistance. However, when ions formed during the electrochemical reaction move from the anode to the cathode and vice versa, an electric current is created. This increase in current can disrupt and break down the passive oxide layer, compromising the protective barrier. As a result, the corrosion resistance of AA6061-T6 decreases, allowing the material to be more susceptible to further corrosion.

The electrode potential of Al^{3+} is lower than that of Fe^{2+}, which makes AA6061-T6 more susceptible to corrosion. Additionally, the presence of Fe particles reduces the localized corrosion resistance of the alloy, meaning that AA6061-T6 undergoes dissolution at the cathode. Metal particles, such as Fe, embedded in the AA6061-T6 matrix, influence its corrosion behavior.

At the interface between AA6061-T6 and SUS316, numerous corrosion cells are formed due to the presence of IMC like Fe_3Al and $FeAl_3$. As a result, corrosion of the weld occurs primarily in the AA6061-T6 sheet, focusing around the IMC layers. This localized corrosion can weaken the weld and reduce its overall performance.

CHAPTER 3. RESEARCH AND EXPERIMENTAL METHODS

3.1. Research method

In this study, the welding speed is varied from 50 mm/min to 250 mm/min, the rotation speed from 600 rpm to 900 rpm, pin length from 2.7 mm to 3.0 mm and the penetration is investigated from 0.20 mm to 0.35 mm.

Fabrication of specimens according to ASTM standards for the study of the microstructure and microhardness testing of the joint.

Microstructure analysis of the zone using SEM (Scanning Electron Microscope) and EDS (Energy Dispersive X-ray Spectroscopy): This involves examining the grain structure, the thickness of the IMC layer, the diffusion layer, and the interface between the two alloys after tensile testing.

Fabrication of corrosion test specimens after successfully friction stir welding AA6061-T6/SUS316 joints to achieve the highest possible strength.

Corrosion testing of weld specimens in different corrosive environments, including: NaCl concentration (%NaCl), NaCl concentration with applied voltage (%NaCl + voltage), NaCl concentration with applied voltage and temperature (%NaCl + voltage + temperature).

3.2. Experimental materials

In this study, AA6061-T6 with thickness of 3.0 mm and SUS316 with thickness of 1.0 mm according to JIS standard were used.

3.3. FSW process between AA6061-T6 and SUS316

3.3.1. Manufacturing equipment

The joint between AA6061-T6 and SUS316 were fabricated at the FSW lab of Nha Trang University.

3.3.2. Welding tool

Welding tool with threadless cylindrical made from SKD11 steel according to JIS standard. Diameter of the shoulder and the pin are 18 mm and 6 mm respectively, the pin length varies from 2.6 mm to 3.0 mm.

3.3.3. FSW process

The positions of the two materials are shown in Fig. 3.1. To reduce the resistance created by the workpiece and material protrusion.

The welding tool is tilted perpendicular to the workpiece at an angle $\theta = 2^0$.

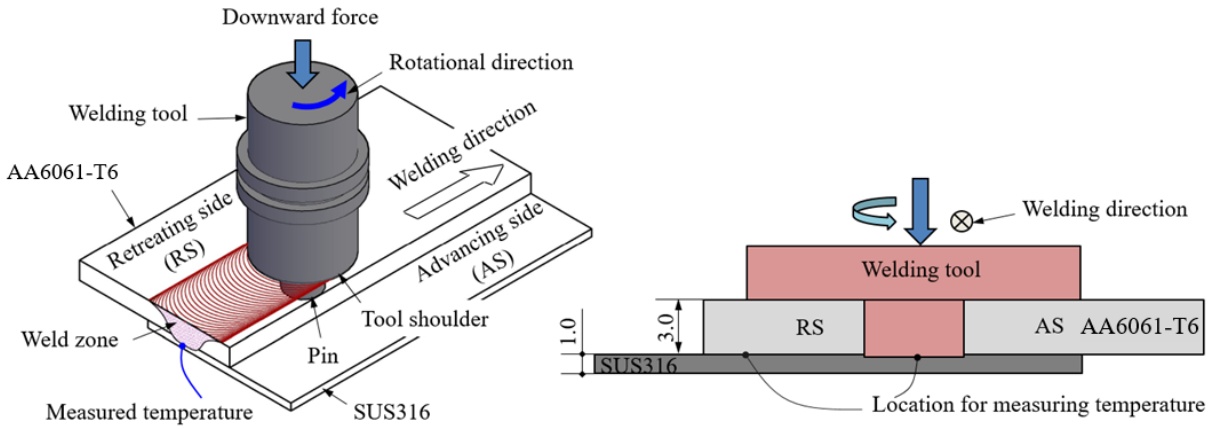

Fig. 3.1. FSW process between AA6061-T6 and SUS316

3.4. Experimental equipment

3.4.1. Measure welding zone temperature

The weld zone temperature was recorded by thermocouple linked to the Graphtec GL240. Location for measuring temperature is shown in Fig. 3.1.

3.4.2. Microstructural analysis around the weld zone

The specimen was polished with Sankyo sandpaper from 1000 to 4000 combined water on the MA-PO250 machine. Then, the specimen was polished with a cloth containing Al_2O_3 alumina. Finally, the sample was etched with Keller's solution.

3.4.3. Lap-joint surface properties

Broke surface after testing and properties of the intermetallic compounds affect the strength of the joint greatly, which are shown in detail through scanning electron microscopy (SEM) and X-ray spectroscopy (EDS).

3.4.4. Microhardness distribution around the weld zone

Investigation of microhardness along the thickness and cross section of the joint. Microhardness was measured by Vickers MMT-X1 device, (Matsuzawa - Japan), under a measuring load of 200 g, load time of 10 seconds according to ASTM E92.

3.4.5. Strength and destructive behavior of the joint

Testing process was performed Instron 3366 at the tensile speed of 2.0 mm/min according to ASTM E8 standard. The machine connects computer to output graphs and tensile force when the specimen is broken.

3.4.6. The influence of corrosive environment on the destruction process

3.4.6.1. Specimen preparation and corrosion rate calculation

Electrochemical corrosion specimen dimensions according to ASTM G71-81 and G31-72. To determine corrosion rate, the joint should be cleaned and subjected corrosion according to ASTM G1. Corrosion rate in different corrosive environments were determined by the gravimetric method.

3.4.6.2. Corrosive environments

- The specimen was immersed in 4 NaCl solutions with different concentrations: 0 %, 1.5 %, 3.0 % and 4.5 %NaCl. The mass and structure after corrosion are checked once a month periodically with 3 checks.

- The specimen was immersed in 3.0 %NaCl solution under different voltages of 3 V, 4 V and 5 V. The mass and structure after corrosion are checked every 30 minutes, 5 times.

- The specimen was immersed in a 3.0 %NaCl solution, the voltage was 3 V and the temperatures varied from 30 ^{o}C - 100 ^{o}C. The mass and structure after corrosion are checked every 30 minutes, 5 times.

CHAPTER 4. RESEARCH RESULTS

4.1. Interaction between welding speed and penetration on the joint properties

4.1.1. Welding zone temperature

Penetration increase from 0.20 mm to 0.35 mm, temperature increase about 20 ^{o}C. Welding speed affects temperature significantly.

The peak temperature decrease about 80 ^{o}C when the welding speed increase from 100 mm/min to 200 mm/min at penetration of 0.20 mm. Similar findings were reported by Mahto et al. Maximum value approximately 500 ^{0}C at welding speed of 100 mm/min, penetration of 0.35 mm. Welding speed affects temperature more than penetration.

4.1.2. Microstructural development

As shown in Fig. 4.1(a), the joint is not defects such as cracks, grooves, and holes. Steel fragments are dispersed in the SZ of aluminum as shown in Fig. 4.1(b, c, d).

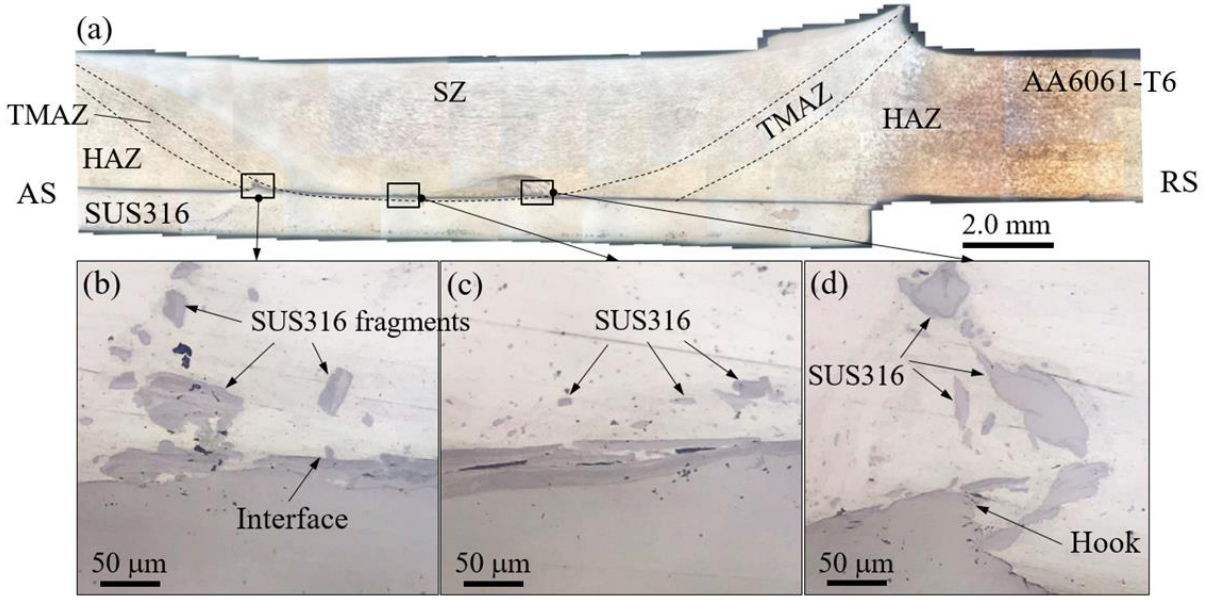

Fig. 4.1. (a) Macrostructure and (b, c, d) microstructure of the specimen at welding speed of 100 mm/min, penetration of 0.35 mm

Increasing welding speed results in a decrease in the IMC thickness. IMC thickness is 2.1 µm at welding speed of 100 mm/min. Meanwhile, the thickness of IMC decrease to 0.6 µm at welding speed of 250 mm/min. Highest thickness value is 6.25 µm at welding speed of 100 mm/min, penetration of 0.35 mm. In addition, the thickness of IMC increase with increasing penetration. Increasing penetration or decreasing welding speed will increase thickness of the IMC and diffusion.

4.1.3. Microhardness distribution

Welding speed and penetration do not affect the microhardness of AA6061-T6 greatly. However, the hardness of SUS316 at SZ increase rapidly, due to the pin strong stirring. Higher hardness value of SUS316 at SZ due to the fine, small grain structure of the IMC. Maximum hardness reaches 260 HV with penetration of 0.35 mm and 150 mm/min welding speed.

4.1.4. Tensile strength and fracture behavior of joint

Displacement is sensitive to welding speed and penetration. When welding speed is low, tensile strength will be high at penetration of 0.30 mm. At penetration of 0.35 mm, lap-joint strength is high when welding speed is increased. Highest tensile strength is about 6,231 N at penetration of 0.30 mm, welding speed of 150 mm/min as shown in Fig. 4.2(b).

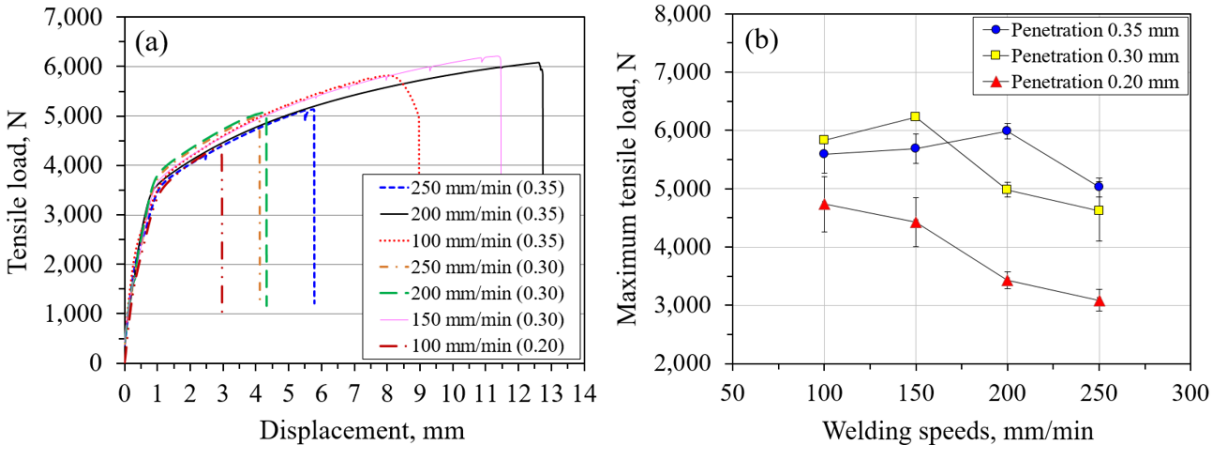

Fig. 4.2. Effect of welding parameters on (a) displacement and (b) tensile strength

The area is 53 mm^2 at welding speed of 150 mm/min and penetration of 0.30 mm. The area reaches 49 mm^2 at penetration of 0.35 mm, welding speed of 200 mm/min. Fracture of the joint at the HAZ on AA6061-T6 when welding speed is 100 mm/min with both penetration of 0.30 mm and 0.35 mm. Maximum area is 60 mm^2 approximately.

4.2. Interaction between welding speed and rotational speed on weld properties

4.2.1. Temperature of weld zone and surface

The highest temperature of 515 ^oC was achieved at a welding speed of 50 mm/min. This temperature drops to 401 ^oC at 200 mm/min. The maximum temperature difference between the HAZ and SZ is approximately 100 ^oC in all cases.

The welded surface is smooth and no defects such as grooves or cracks. Significant material extrusion defect was observed at welding speed of 50 mm/min.

4.2.2. Cross section of the joint

Due to the difference temperature, the grain growth of the weld zones is not uniform. The grain size increases from SZ to HAZ corresponding to the decrease in stirring. Reduction in IMC thickness due to increased welding speed. The IMC thickness along interface is not uniform. IMC was not detected at 200 mm/min. Longitudinal crack at the interface indicated AA6061-T6 did not bond SUS316.

4.2.3. Microhardness distribution

Hardness of the HAZ on AA6061-T6 decreased and expanded correspondingly welding speed decrease as shown in Fig. 4.3(a). High temperature causes coarse grain structure of AA6061-T6, so hardness is reduced. The hardness of SZ on SUS316 is very high at 50 mm/min and 75 mm/min.

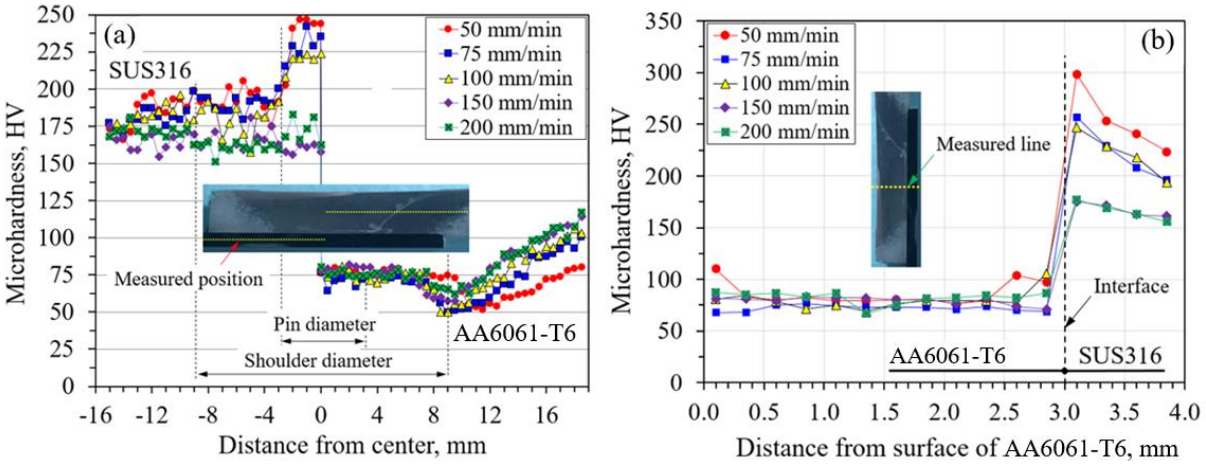

Fig. 4.3. Microhardness distribution (a) cross - section (b) thickness at different welding speeds

The hardness of SUS316 is more sensitive to rotation speed. Highest hardness is approximately 282 HV at 900 rpm. The results showed that increasing the rotation speed will increase microhardness.

4.2.4. Tensile strength and fracture behavior of joint

The stress - strain curves depend on welding speed significantly, especially tensile strength of the joint. As shown in Fig. 4.4(b), highest tensile strength about 5,506 N, decreasing sharply when the welding speed increases from 75 mm/min to 200 mm/min.

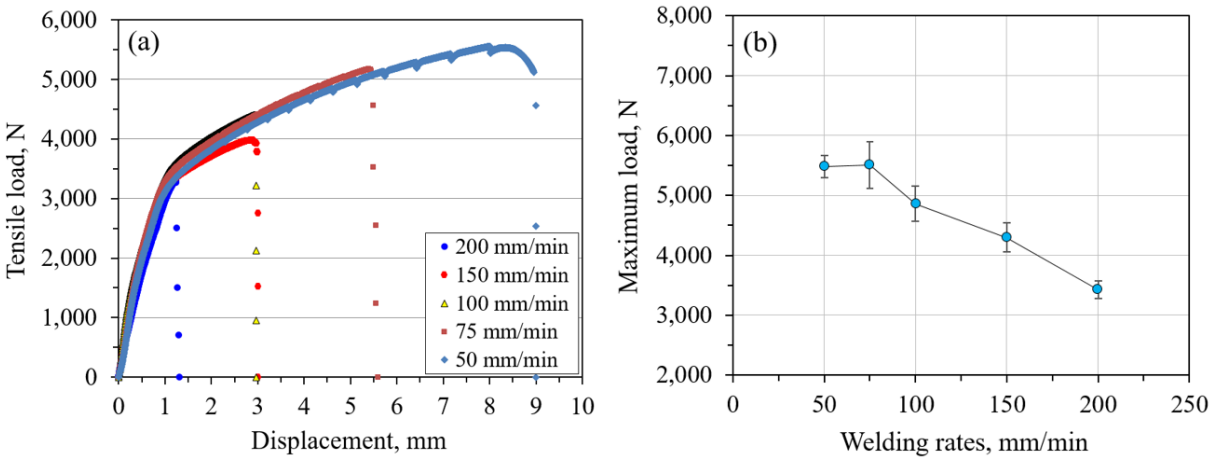

Fig. 4.4. (a) Stress - strain curves and (b) tensile strength of AA6061-T6/SUS316 at different welding speeds

Highest strength approximately 6,228 N at 700 rpm, with welding speed of 200 mm/min, and 0.30 mm penetration. As the rotational speed increase to 900 rpm, the tensile strength decrease, reaching a value of about 6,055 N. The tensile strength is influenced by properties of the IMC and the stirring efficiency of the pin.

Maximum area is 60 mm^2 at 75 mm/min. The area decrease sharply when the welding speed increase from 75 mm/min to 200 mm/min. At a rotation speed of 700 rpm, the estimated area is 60 mm^2 approximately. The bonding area is similar, about 34 mm^2 at 600 rpm and 800 rpm.

4.3. Interaction between pin length and penetration on the joint properties

4.3.1. Weld surface

The joint was fabricated with pin length varying from 2.7 mm to 3.0 mm, rotation speed of 800 rpm, welding speed of 200 mm/min and penetration of 0.30 mm as fixed constants. Smooth welding surface, no burrs, cracks with pin length of 2.7 mm. The joint with burr defect was formed significantly at pin length of 2.9 mm.

4.3.2. Microstructural development

The joint is made with pin length of 2.9 mm, no defects such as cracks, grooves, and holes as shown in Fig. 4.5(a). The aluminum size varies across the weld zones. Grain size increases from SZ to TMAZ respectively (Fig. 4.5(b, c, d)). Different temperature distribution results the grain size around the weld zone.

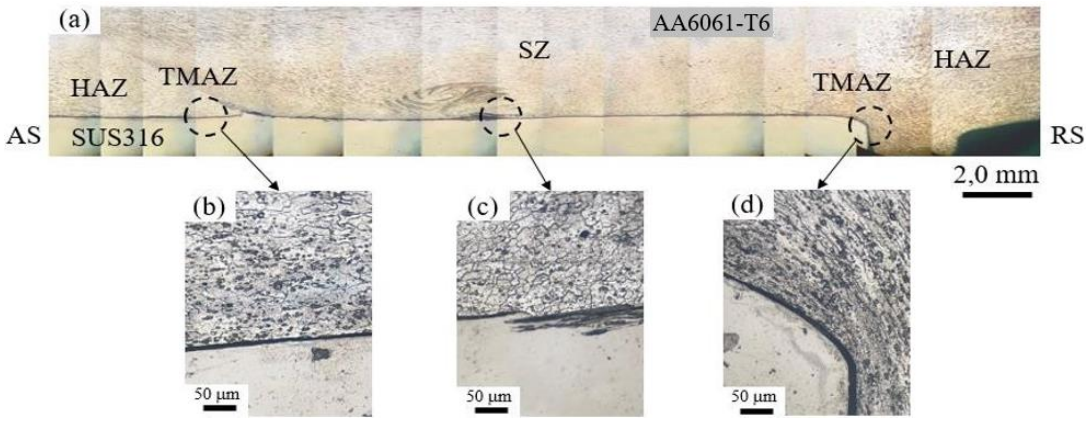

Fig. 4.5. (a) Macrostructure and (b, c, d) microstructure of the specimen at 800 rpm, 200 mm/min and 0.30 mm

4.3.3. The joint surface properties

IMC thickness is about 0.12 µm at pin length of 2.9 mm, penetration of 0.20 mm. Pin length decreases to 2.7 mm without forming IMC, although the penetration increases to 0.40 mm. Apparently, AA6061-T6 is bonded SUS316 well when the pin length increase. The diffusion thickness reached 4.10 µm at pin length of 2.9 mm and penetration of 0.20 mm. Meanwhile, the diffusion thickness increases to 6.10 µm at 0.30 mm penetration. The results confirm that increasing the IMC thickness will increase the thickness of the diffusion.

4.3.4. Microhardness distribution

Penetration and pin length do not affect microhardness of AA6061-T6 on the thickness greatly. The hardness of AA6061-T6 increases rapidly with increasing pin length, while decreasing on SUS316 cross section sharply.

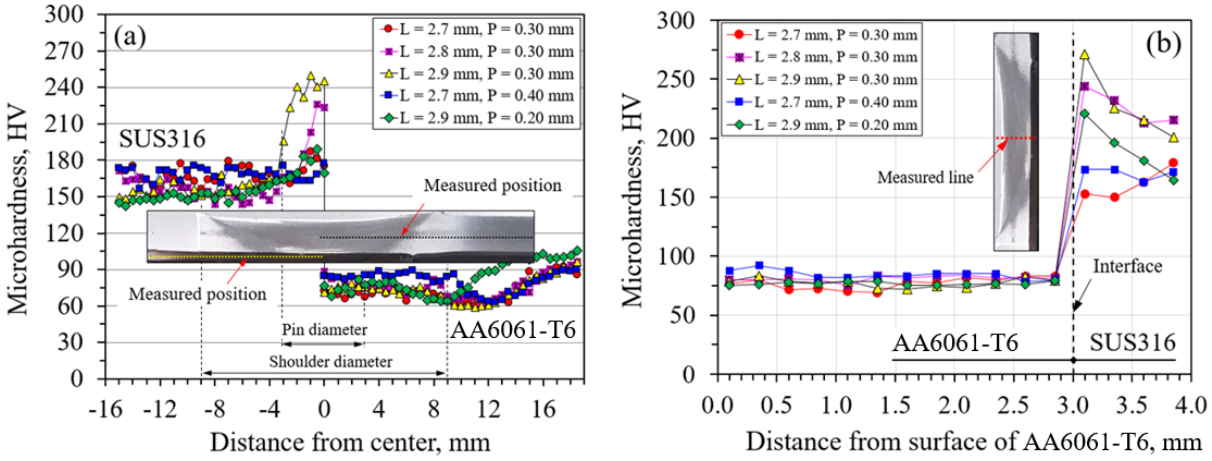

Fig. 4.6. Effect of pin length and penetration on microhardness (a) cross section, (b) thickness of the AA6061-T6/SUS316 lap-joint

It shows that, with small penetration, heat input is low so grain size of the SZ is large. As shown in Fig. 4.6, maximum hardness reached 250 HV at cross section and 271 HV at thickness of the joint with penetration of 0.30 mm, and pin length of 2.9 mm.

4.3.5. Tensile strength and fracture behavior of joint

As Fig. 4.7, Tensile strength of the joint is low at penetration of 0.20 mm and 2.8 mm pin length. The tensile strength increases with increasing penetration. The pin length determines mechanical properties than the penetration. Maximum tensile strength reaches approximately 6,425 N when the pin length increases to 3.0 mm, while the penetration is as small as 0.20 mm. Penetration and pin length increase simultaneously, the tensile strength increases rapidly. Maximum tensile strength is 6,526 N approximately at penetration of 0.30 mm and pin length of 2.9 mm.

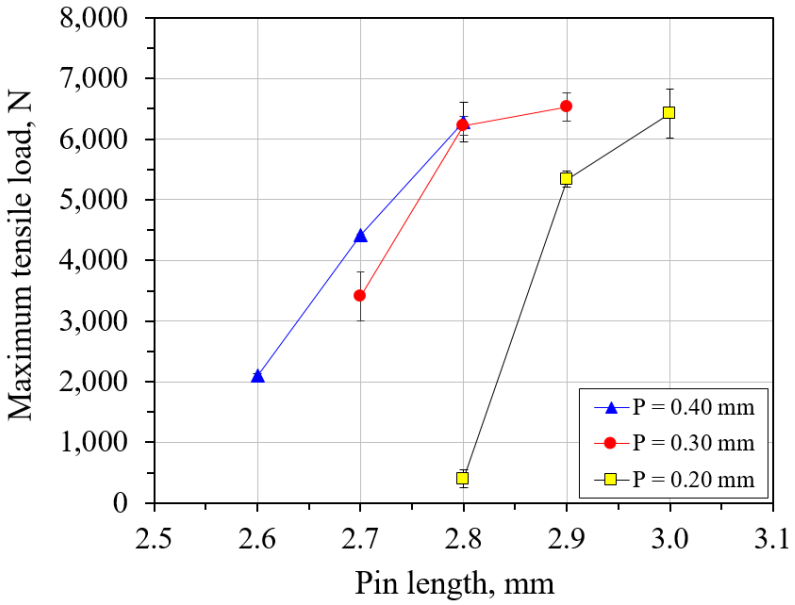

Fig. 4.7. Effect of penetration and pin length on tensile strength

Minimum area is about 24 mm^2 when the pin length is 2.7 mm. Maximum area is 60 mm^2 approximately at pin length of 2.9 mm, 0.30 mm penetration. The lap-joint is broken at HAZ on AA6061-T6. Results showed that the bond between AA6061-T6 and SUS316 increase with increasing pin length, so tensile strength of the joint increases. Heat input and stirring action of the pin form a bond between AA6061-T6 and SUS316. The joint is fabricated with penetration of 0.20 mm and pin length of 3.0 mm, showing large number indentations. This means that the two alloys bond well but increase penetration can create a rough and brittle bond interface.

4.4. Effect of NaCl solution on corrosion process

4.4.1. Destruction structure

Results showed uniform corrosion on all surfaces, increasing with time and %NaCl when the specimen was immersed in NaCl solution for 30 days. Immersion time is 90 days, the dark oxide layer cover the AA6061-T6 corrosion spots and the surface, thus hindering corrosion process.

4.4.2. Corrosion rate

Maximum corrosion reached 8 mg when immersed in 4.5 %NaCl solution after 30 days. Corrosion mass is large during the first 30 days of immersion, and small during next immersions, about 1 mg. Corrosion rate increases as %NaCl increases in Fig. 4.8.

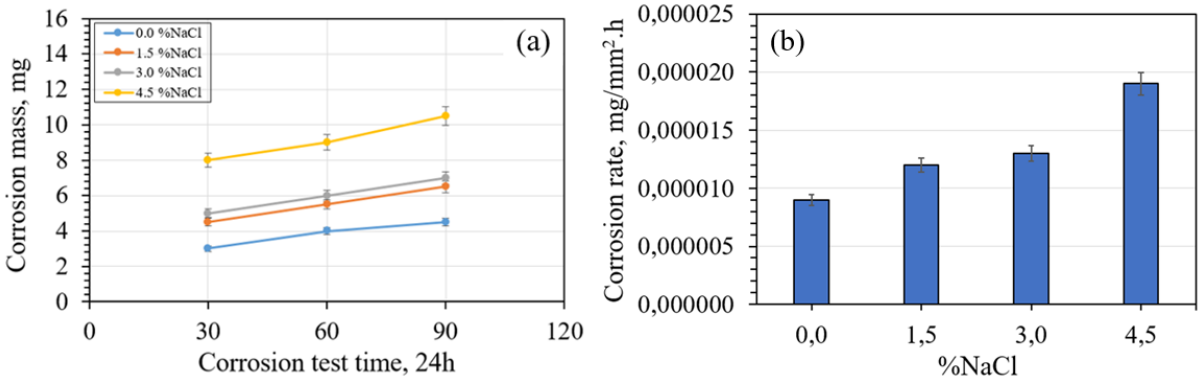

Fig. 4.8. Corrosion of AA6061-T6/SUS316 in different %NaCl solutions (a) corrosion mass - mg, (b) corrosion rate - mg/mm^2.h

4.4.3. Corrosion mechanism analysis

AA6061-T6 reacts strongly with H_2O, leading to the continuous formation of the $Al(OH)_3$ oxide layer on the corroding surface. After soaking the sample for 30 days and nights, corrosion of the AA6061-T6 joint starts to appear, with the formation of a passive oxide layer, as shown in Fig. 4.9. The $Al(OH)_3$ layer is thin and sparse, which limits the corrosion resistance.

After soaking the sample for 90 days, a thicker layer of aluminum hydroxide $Al(OH)_3$ forms around the corrosion sites. This passive $Al(OH)_3$ layer plays a role in reducing the corrosion of AA6061-T6, as illustrated in Fig. 4.10 and Fig. 4.11. The increased thickness and presence of the $Al(OH)_3$ layer improve the material's resistance to further corrosion.

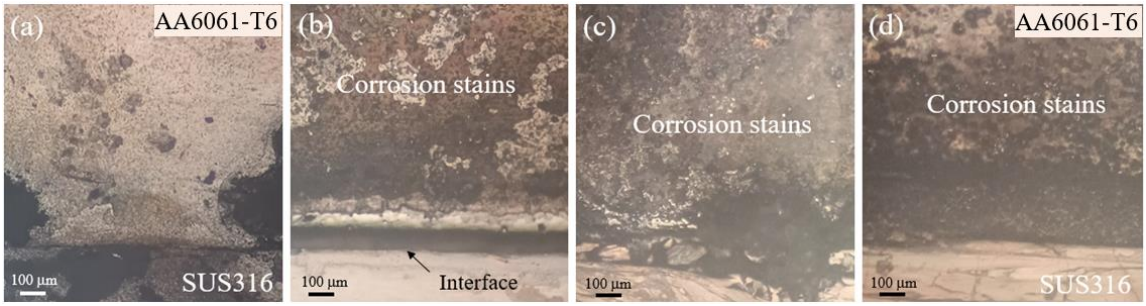

Fig. 4.9. Corrosion structure of the lap - joint at the SZ after 30 days soaked in NaCl solution (a) 0 %NaCl, (b) 1.5 %NaCl, (c) 3.0 %NaCl, (d) 4.5 %NaCl

Under the influence of Cl^- ions, the passive oxide layer is destroyed quickly, and a new oxide layer forms immediately. Since the protective oxide layer is dissolved, AA6061-T6 begins to dissolve, which increases the corrosion rate. The width of the corrosion at the interface increases from 30 µm to 100 µm as the NaCl concentration increases from 0.0 % to 4.5 % (Fig. 4.10). As a result, the depth and extent of corrosion are greater in AA6061-T6.

Furthermore, uniform corrosion occurs in the TMAZ because the grain size in this area is coarser than that in the SZ. This leads to a greater susceptibility to corrosion in the TMAZ, where the microstructure is less refined compared to the SZ.

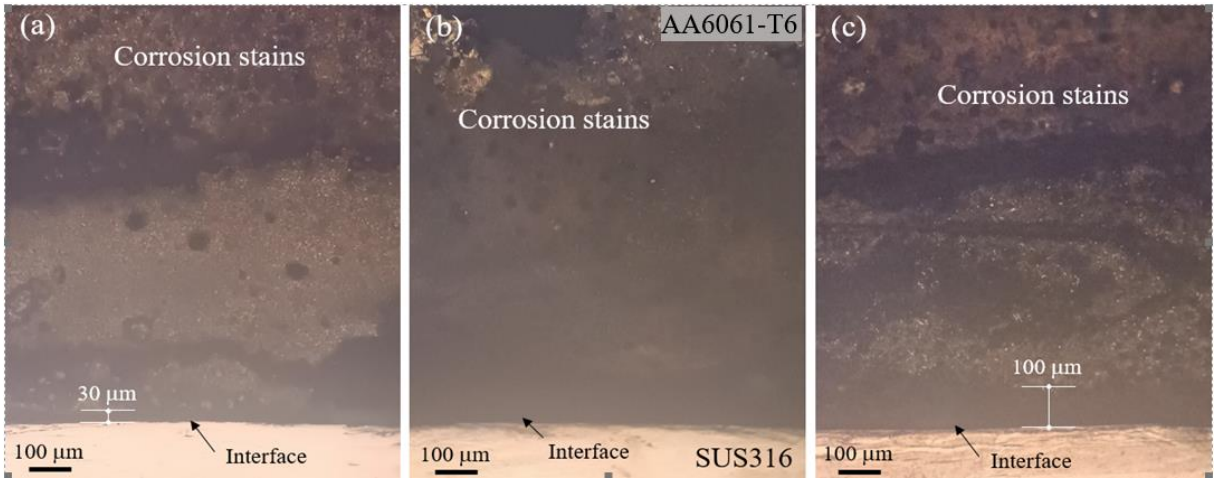

Fig. 4.10. SZ microstructure of specimen after 90 days in different NaCl solution (a) 0 %NaCl, (b) 1.5 %NaCl, (c) 4.5 %NaCl

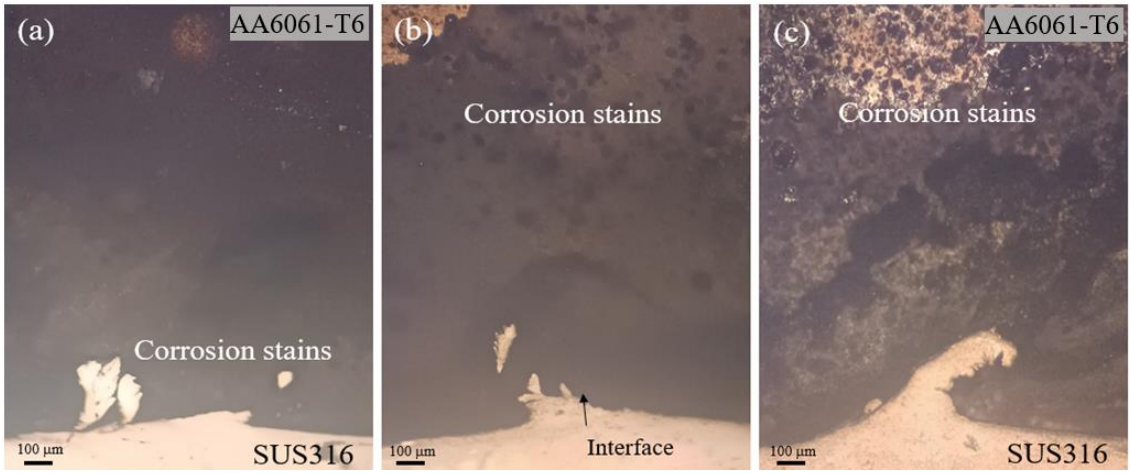

Fig. 4.11. Near SZ microstructure of specimen after 90 days in different NaCl solution 0 %NaCl, (b) 1.5 %NaCl, (c) 4.5 %NaCl

4.5. Effect of voltage on corrosion process

4.5.1. Destruction structure

The AA6061-T6/SUS316 lap-joint immersed in 3.0 %NaCl solution under the 3 V, 4 V, 5 V voltage. Corrosion microstructure of SZ under the influence of different voltages as shown in Fig. 4.12.

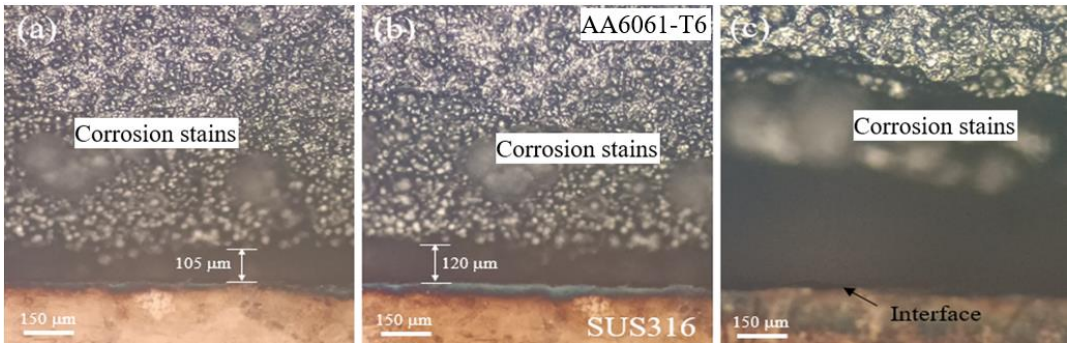

Fig. 4.12. SZ microstructure at different voltages (a) 3 V, (b) 4 V, (c) 5 V

4.5.2. Corrosion rate

Under the influence of different voltages, corrosion is different, especially at the interface between AA6061-T6 and SUS316. Maximum corrosion mass is 49 mg with voltage of 5 V, corresponding to corrosion rate of 0.0400 mg/mm^2.h.

Voltages	3 V	4 V	5 V
Corrosion rate (mg/mm^2.h)	0.0150	0.0217	0.0400

4.5.3. Corrosion mechanism analysis

Uniform corrosion on the AA6061-T6 when the voltage is 3 V as shown in Fig. 4.12(a). In Fig. 4.12(b, c), severe corrosion forming large patches when increasing

voltage. Corrosion size on AA6061-T6 and the interface increases with increasing voltage. Under electric current, AA6061-T6 is corroded, forming ions Al^{3+} that move from the cathode to the anode $Al = Al^{3+} + 3e$. Then $Al^{3+} + 3H_2O = Al(OH)_3 + 3H^+$. When the voltage increases, more Al^{3+} ions are formed, so the corrosion rate of AA6061-T6 increases. The potential difference between the IMC particles and the AA6061-T6 basic forms corrosive cells. Therefore, aluminum dissolves in NaCl solution continuously as the voltage increases.

4.6. Effect of temperature on corrosion process

4.6.1. Destruction structure

Corrosion structure of the AA6061-T6/SUS316 joint immersed in 3.0 %NaCl solution, voltage of 3 V and temperature of 70 ºC as shown in Fig. 4.13.

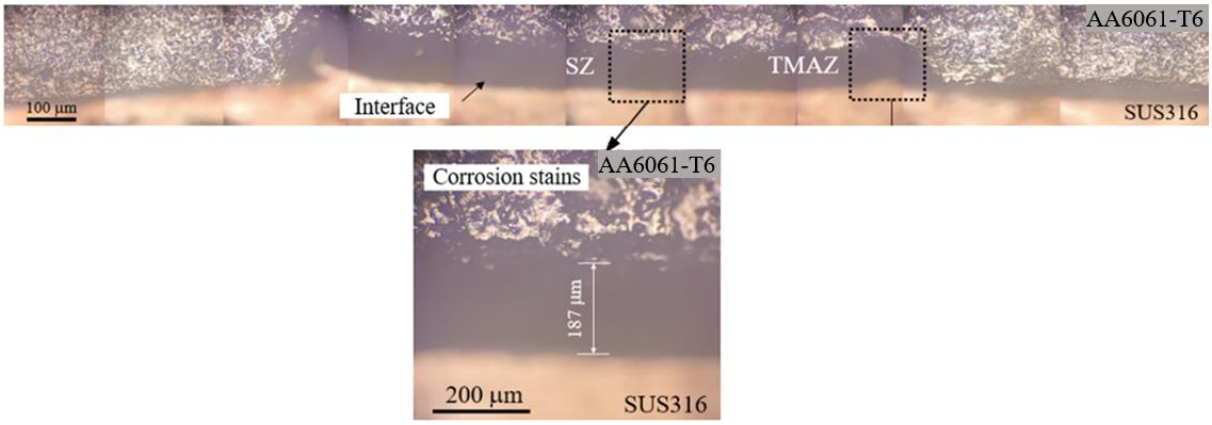

Fig. 4.13. Cross section of the AA6061-T6/SUS316 joint corrosion at 70 ºC

Corrosion of the lap-joint at SZ with temperature of 50 ºC, 80 ºC and 100 ºC in Fig. 4.14.

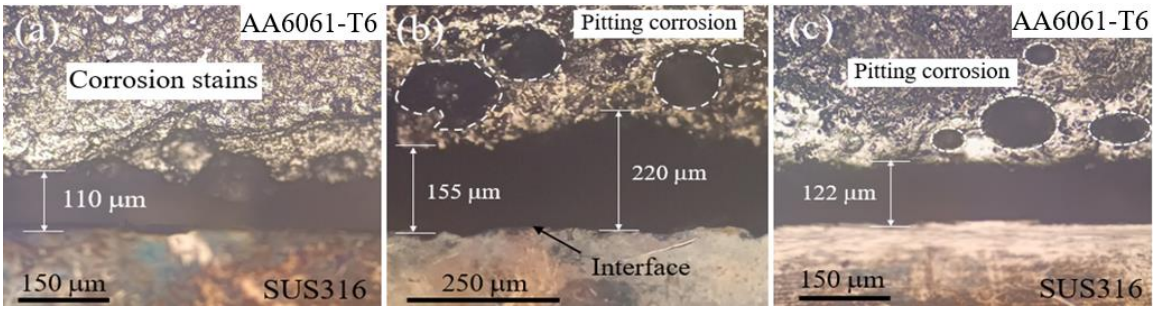

Fig. 4.14. Corrosion microstructure of SZ at temp (a) 50 ºC, (b) 80 ºC, (c) 100 ºC

4.6.2. Corrosion rate

The corrosion rate increases from 30 ºC to 60 ºC. Conversely, as the temperature increases from 70 ºC to 100 ºC, the corrosion rate decreases.

Temperature (°C)	30	50	60	70	80	100
Corrosion rate (mg/mm^2.h)	0.0150	0.0776	0.0922	0.1257	0.0421	0.0346

4.6.3. Corrosion mechanism analysis

As the temperature increases from 30 °C to 70 °C, the rate of chemical corrosion reaction increases continuously (Fig. 4.13 và Fig. 4.14). The passive film $Al(OH)_3$ form on the AA6061-T6 is small relatively and the structure is not stable. It means that corrosion is uniform and the corrosion rate increases continuously as temperature increases. When the temperature is greater than 70 °C, the chemical corrosion reaction increase. However, the passive film $Al(OH)_3$ structure was stable and increased. The passive oxide functions to reduce corrosion. Therefore, the corrosion rate decreases when the temperature is greater than 70 °C. The temperature increased to 80 °C as shown in Fig. 4.14(b), some incomplete passive film absorbed ions Cl^-, so the AA6061-T6 dissolved high rate, forming holes, causing pitting corrosion. The pitting corrosion size at IMC decrease as the temperature increase, especially the corrosion spots on AA6061-T6 (Fig. 4.14(c)).

CHAPTER 5. CONCLUSION AND RECOMMENDATIONS

5.1. Conclusion

Welding speed affects the temperature significantly. As the welding speed increases, the welding temperature in the HAZ and SZ decreases. On the other hand, the penetration does not have a significant effect on the welding temperature.

Dispersed SUS316 particles were detected in the SZ of AA6061-T6 due to the increased penetration, which causes the pin to come into the SUS316 surface.

Welding temperature significantly affects the formation and thickness of the IMC and the diffusion layer. Increasing the penetration or reducing the welding speed leads to an increase in the thickness of both the IMC and diffusion layer.

Reducing the welding speed and increasing the penetration are beneficial for mixing the two alloys, but they lead to coarser grain size and fracture occurring at the HAZ on the AA6061-T6.

The tensile strength is influenced by both the thickness of the IMC layer, the diffusion layer, the characteristics of the IMC layer, and the stirring efficiency of the pin, which are reflected in both the interface and the bond area.

High input heat will form a thick and brittle IMC layer, resulting in a larger bond area between AA6061-T6 and SUS316. Conversely, low input heat leads to a smaller bond area, which reduces the tensile strength of the joint.

Mcirohardness decreases as welding speed decreases, especially in the HAZ of AA6061-T6 due to coarser grain structure. Additionally, welding speed has little impact on the hardness of AA6061-T6, but the hardness value of SUS316 in the SZ increases rapidly.

Corrosion occurs most severely in the SZ and TMAZ when immersed in NaCl solution, especially at high concentrations. The microstructural inhomogeneity of the welded areas is the main cause of this corrosion.

Corrosion increases as the voltage is raised from 3V to 5V, particularly at the interface. Higher voltage enhances the Cl^- ion migration process, making it easier to break down the $Al(OH)_3$ layer.

The corrosion reaction rate increases with temperature, reducing the protective capability of the $Al(OH)_3$ passive oxide layer. However, at temperatures above 70 °C, the oxide film structure becomes unstable, absorbing Cl^- ions and forming corrosion

pits. As a result, localized pitting corrosion occurs, leading to a decrease in the overall corrosion rate.

5.2 Recommendations

5.2.1. Limitations of the topic

Besides the thickness of the IMC layer, the diffusion layer, and the bonding characteristics between AA6061-T6 and SUS316, these factors will also affect the mechanical properties. Therefore, the phases of the IMC layer at the interface have not been determined yet.

High input heat will form a thick and brittle IMC layer. However, the phases of the thick IMC layer have not been determined yet. Based on the references of Newishy M. et al. (2023) and Xingbin H. et al. (2024), it can be predicted that the IMC layer will be thick and brittle.

The bonding characteristics and the bond area affect the tensile strength, but the influence of specific phases on the bonding has not been determined yet.

The phases of the IMC layer affect the electrochemical corrosion at the interface. The tensile strength under different corrosive environments has not been evaluated yet.

5.2.2. Recommendations

The study of the lifetime and failure mechanism of the AA6061-T6/SUS316 lap-joint under cyclic loading over time.

Research of the tensile strength in high temperature environments.

The study of the effect of NaCl, NaCl + voltage, and NaCl + voltage + temperature on the tensile strength. Comparison of the tensile strength of the AA6061-T6/SUS316 lap-joint before and after corrosion.

Taking X-Ray diffraction of the interface to identify the phases of the IMC layer. From there, determining whether the IMC layer is rich in Fe or Al, and how the oxide phases affect the mechanical properties of the lap-joint.

The EDS scan is conducted to determine the phases of the IMC layer at the interface when the lap-joint is made at different pin lengths.

Replace the current NaCl solution with a natural seawater environment.

Replace the F48000 furnace with another heating device.

Study the influence of the phases of the IMC layer on electrochemical corrosion in NaCl, NaCl + voltage, and NaCl + voltage + temperature environments.

LIST OF AUTHOR'S PUBLISHED WORKS

1. **Huy HH**., Hao DD., Nam QH. and Tra HT. (2024). “Welding speed and pin penetration interaction in mechanical properties of friction stir welded lap-joint AA6061/316 stainless steel”, Journal of Materials Engineering and Performance. https://doi.org/10.1007/s11665-024-09747-2 (SCIE-Q2).
2. **Huy HH**., Quan MN., Thuyen CP., Hao DD., Tra HT. (2024). “Effect of probe length on tensile strength of dissimilar friction stir welded lap-joint between AA6061 and 316 stainless steel using marine structure”. Journal of Fisheries Science and Technology, No.1, pp. 089 - 094. https://doi.org/10.53818/jfst.01.2024.254.
3. **Huy Huu Ho** (2024), “Impact of NaCl concentration on the dissimilar friction stir welded lap-joint AA6061/SUS316 corrosion behavior”, Proceedings of the International Scientific Conferences (ISC) 2024 “Green Values for Sustainable Development”, pp. 725 - 729.
4. **Huy HH**., Hao DD., Quan MN., Tra HT. (2023), “Assessment of dissimilar friction stir welded AA6061/SS316 for sustainable industry”, International Conference MSDI 2023. IOP Conf. Ser.: IOP Conference Series: Earth and Environmental Science. 1278 012025. DOI 10.1088/1755-1315/1278/1/012015 (Scopus).
5. **Huy HH**., Hao DD., Quan MN., Tra HT. (2023), “Mechanical performance of dissimilar friction stir welded lap-joint between aluminum alloy 6061 and 316 stainless steel”, Welding International, 37(2), pp.101 - 110. https://doi.org/10.1080/09507116.2023.2190475 (Scopus).
6. **Huy HH**., Hao DD., Nam HQ., Thuyen CP., Tra HT. (2022), “Dissimilar Friction Stir Welded lap-joint of Aluminum Alloy 6061 and 316 Stainless Steel”, 6th International Conference GTSD 2022, pp. 165 - 168.